Drag Reduction by Strakes of Noncircular Cylinders

B. N. Pamadi* and C. Pereira†
Indian Institute of Technology, Bombay, India
and
B. H. Laxmana Gowda‡
Indian Institute of Technology, Madras, India

An experimental investigation is conducted to evaluate the effect of strakes on the crossflow drag coefficient of a typical noncircular cylinder at subcritical Reynolds numbers. The strake height and, more particularly, its location on the windward face, has a strong influence on the flow pattern, base pressure, and drag coefficient. Substantial drag reductions of the order of 80% are found to be possible by this technique.

Nomenclature

b_o = width of the model
C_p = pressure coefficient $= \dfrac{p - p_\infty}{\frac{1}{2}\rho V^2}$
C_{pb} = average base pressure coefficient
C_D = drag coefficient $= \dfrac{\text{drag force per unit length}}{\frac{1}{2}\rho V^2 b_o}$
C_{DO} = drag coefficient of basic model (no strakes)
h = height of strake
k = nondimensional corner radius $= r^*/b_o$
r = distance measured along the bottom surface from corner to strake location
r^* = corner radius
V_∞ = freestream velocity
θ = angle measured counterclockwise to a given point on the model surface from the stream direction
ε = nondimensional height of the strake $= h/b_o$
η = nondimensional strake location $= r/b_o$

Subscript

∞ = freestream

Introduction

THE subject of drag reduction has always attracted the attention of aerodynamicists. This problem has assumed greater importance in recent years on account of escalating cost of energy.

The drag of two-dimensional bluff bodies consists mainly of pressure drag, skin friction forming only a small and insignificant part of the total drag. At subcritical Reynolds numbers, the flow over bluff bodies is characterized by a large wake and periodic, alternate vortex shedding. The separated shear layers feed vorticity to these alternating vortices that are continuously shed downstream. With this flow pattern, the time-averaged pressure drag coefficient assumes very large values and often exceeds the flat plate drag coefficient of 2.0. This fact is particularly true for noncircular cross sections with sharp corners.[1,2,3]

As Reynolds numbers increase beyond the critical value, a transition occurs in the separated shear layer and the flow reattaches to the body as turbulent boundary layer. This reattached flow continues along the body to some extent but will eventually separate and form a turbulent wake that is much smaller in size compared to the wake at subcritical Reynolds numbers. The vortex-shedding phenomenon is significantly suppressed at supercritical Reynolds numbers and the drag coefficient assumes low values.

A popular method of reducing the drag of sharp-edged bluff bodies at subcritical Reynolds numbers is the rounding of corners. As an example of this technique, let us consider a two-dimensional square cylinder (Fig. 1). At subcritical Reynolds numbers, the drag coefficient of this body ($k = 0$) is around 2.0. With progressive increase in corner radius, the drag coefficient reduces and reaches the limiting value close to 1.0 corresponding to that of the circular cyliner. Thus, the maximum reductions achievable by corner-rounding technique appear to be limited to 50%.

In the present study, we have explored the effect of strakes on the drag coefficient of a typical noncircular cross section with sharp windward corners. Systematic low-speed, wind-tunnel pressure measurements and water-tunnel flow visualization tests have been carried out for various strake configurations. It is found that significant drag reductions, much in excess of that indicated by corner roundings, are possible by this technique.

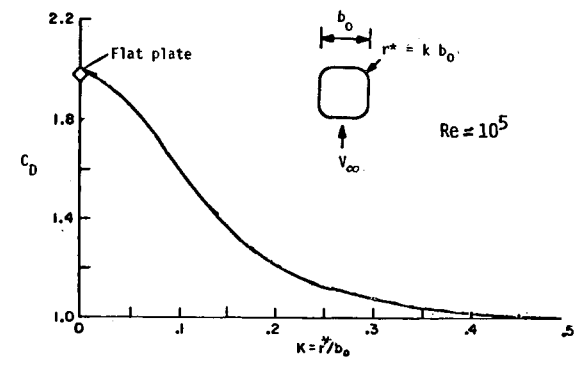

Fig. 1 Effect of corner radius on the crossflow drag coefficient.

Received Dec. 29, 1986; presented as AIAA Paper 87-0360 at the 25th Aerospace Sciences Meeting, Reno, NV, Jan. 12-15, 1987; revision received Aug. 5, 1987.

*Professor, Department of Aeronautical Engineering, currently Research Scientist, Vigyan Research Associates, Inc., Hampton, VA. Member AIAA.
†B. Tech. Student, Department of Aeronautical Engineering.
‡Assistant Professor, Department of Applied Mechanics.

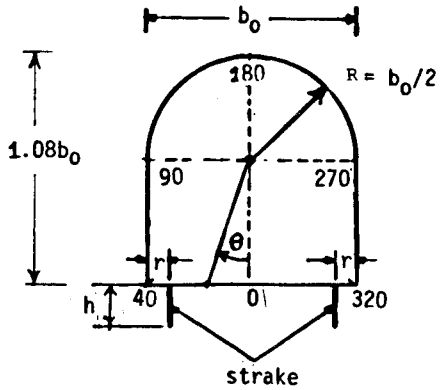

a) Model geometry and strake locations ($h/b_o = 0.1$, 0.2, 0.3; $r/b_o = 0$, 0.1, 0.2, 0.3, 0.4, 0.5)

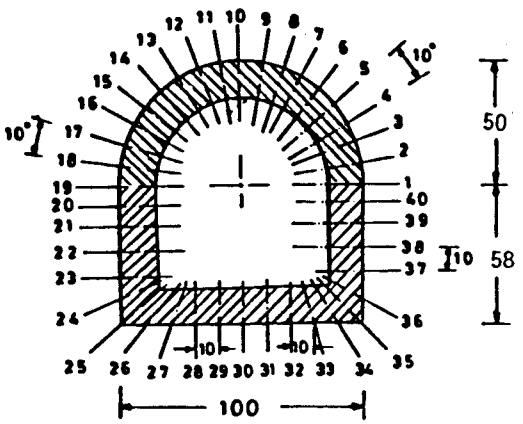

b) Pressure test model (numbers 1–40 refer to pressure tap locations; dimensions in mm)

Fig. 2 Test model.

Experimental Work

Pressure Distribution Tests

These tests were carried out in a 61-cm × 61-cm (2-ft × 2-ft) low-speed, closed-jet, open-circuit wind tunnel having a velocity range up to 35 m/s (115 ft/s). The test model (Fig. 2) was constructed out of well-seasoned teak wood and polished to produce a smooth-surface finish. The test cylinder spanned the horizontal dimension of the wind-tunnel test section. The orifice locations at which pressures were measured are indicated in Fig. 2. Altogether, there are 40 orifices located at the midplane cross section of the test cylinder. Some additional orifices at two other equidistant locations on either side of the midplane were also installed to continuously monitor the existence of a true, two-dimensional flow over the model.

Pressure distribution was measured for basic model (no strakes) and for strakes of heights $\xi = 0.1$, 0.2, and 0.3; and for $\eta = 0$–0.5. Strakes were cut out of thin plastic sheets and rigidly attached to the model with glue. The test Reynolds number based on width (b_o) was in the range 0.5 to 1.1×10^5, which falls in the subcritical range for the subject noncircular section.

Flow Visualization Tests

These tests were carried in a small water tunnel at a velocity of 0.15 m/s. The width (b_o) of the test model was 4 cm. The test Reynolds number based on model width was around 6×10^3. The flow around the model was made visible by the use of aluminum powder employed as tracer medium. Photographs were taken by a 35-mm camera using a sensitive high-speed film. Only two strake heights ($\xi = 0.1$ and 0.3) were employed in these tests. The strake locations were identical to pressure distribution test ($\eta = 0$–0.5).

Results and Discussion

The pressure distributions over the basic model and various strake configurations $\xi = 0.1$, 0.2, and 0.3, located at $\eta = 0$–0.5 are presented in Fig. 3. Notice that the scale for θ is stretched between $\theta = 0$–40 deg and 320–360 deg to bring out clearly the

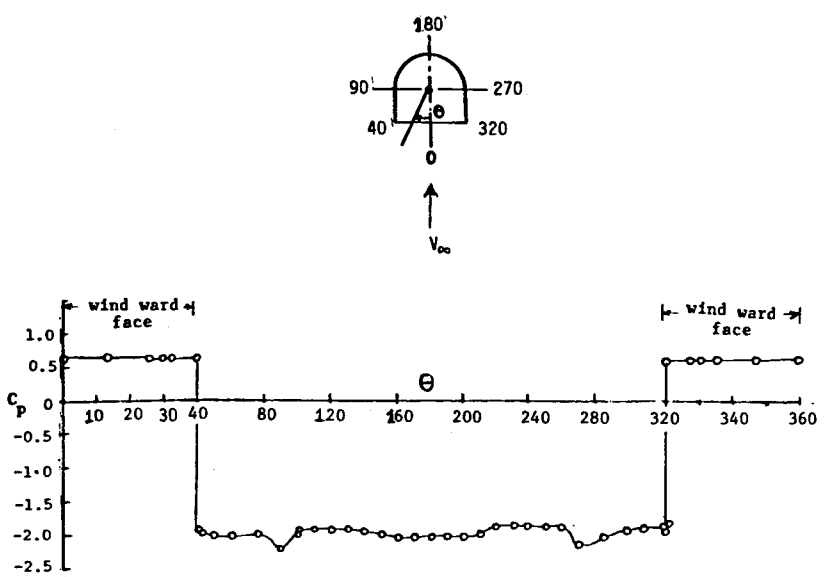

a) Basic model

Fig. 3 Pressure distributions for basic model and various strake configurations (continued on pp. 294 and 295).

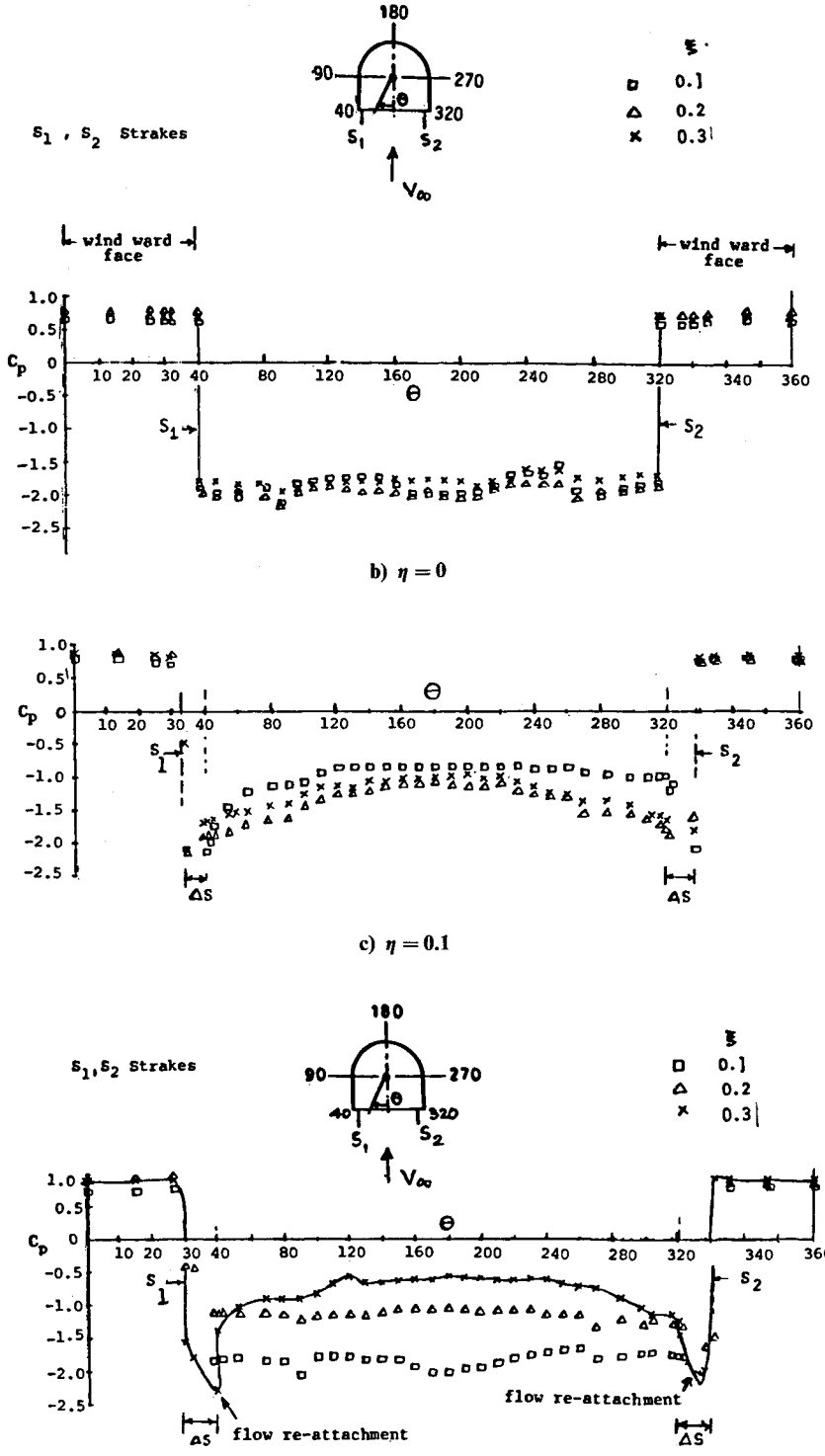

b) $\eta = 0$

c) $\eta = 0.1$

d) $\eta = 0.2$

e) $\eta = 0.3$

Fig. 3 Continued (pressure distributions).

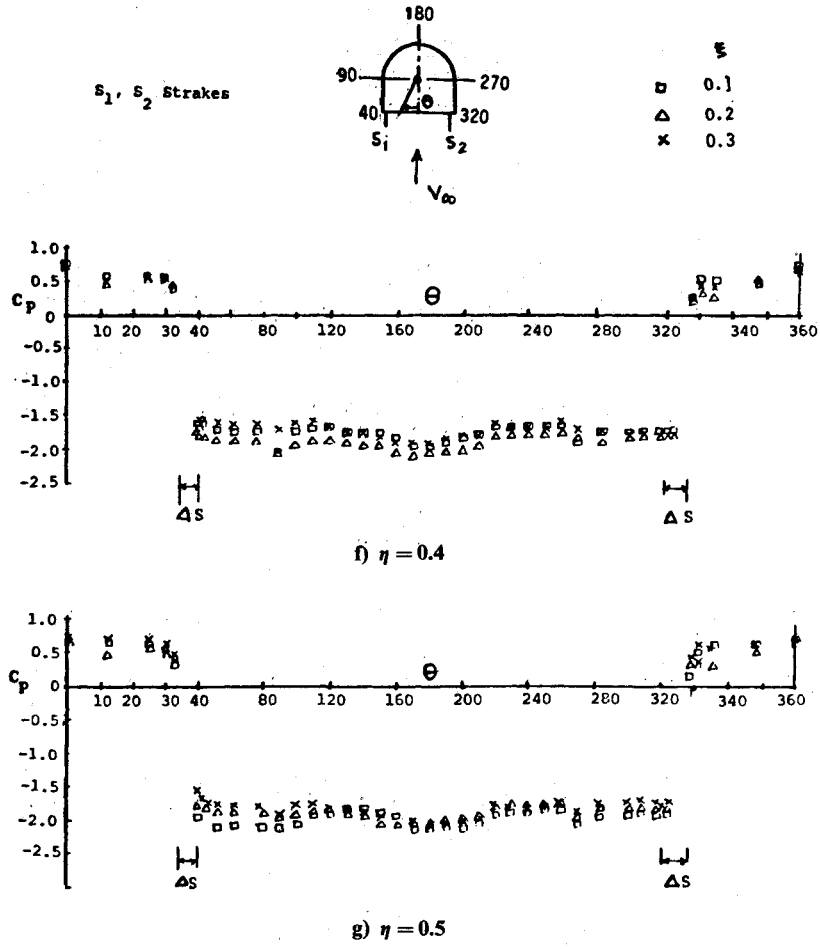

f) $\eta = 0.4$

g) $\eta = 0.5$

Fig. 3 Continued (pressure distributions).

variation of pressure between the strakes and the windward corners. Water-tunnel flow visualization photographs (for $\xi = 0.1$ and 0.3) are presented in Fig. 4. The base pressure coefficient (C_{pb}) and drag coefficients are given in Figs. 5 and 6, respectively.

Basic Model

The basic model has extensive wake, much larger in size compared to the cross-sectional width of the body (Fig. 4a). The wake is characterized by strong alternate and periodic vortex shedding. The wake flow is oscillatory. The separated boundary layers at the sharp corners feed large amounts of vorticity into these vortices, which are shed continuously in downstream direction. This loss of energy appears in the form of a large, time-averaged base suction ($-C_{pb} \simeq 2.0$) and a large drag force on the body ($C_{DO} \simeq 2.2$). The vortex motion has a high degree of coherence and strong periodicity.

Model with Strakes

The installation of strakes at the corners ($r = 0$) apparently does not produce any change (Fig. 4b). However, as the strakes are moved inwards, the base suction ($-C_{pb}$) and C_D start dropping (Figs. 5 and 6). For $\xi = 0.1$, maximum base pressure recovery and minimum C_D occur at $\eta = 0.1$. The corresponding drag reduction is 48%. However, for $\xi = 0.2$ and 0.3, the location of strakes where best results occur in terms of drag reduction is at $\eta = 0.2$. The associated drag reductions are, respectively, 56 and 81% (Fig. 6). The strake configuration ($\xi = 0.3$, $\eta = 0.2$) that gives maximum drag reduction of 81% will be referred to as "optimum configuration." With strakes moved farther inwards, the drag coefficient rises quickly and its value with strakes at $\eta = 0.5$ comes back to that of basic model.

Based on the flow visualization photographs and the pressure distribution data, three different types of flow regimes (Fig. 7) could be identified as follows.

1) Type A: This kind of flow pattern occurs (Fig. 7a) when the strakes are at, or too close, to the corners. In this case, the separated shear layer originating at the edges of the strakes opens out, forming a large wake, and no reattachment of the flow ever occurs. Strong, alternate, periodic vortex shedding continues to occur as observed for the basic model. The drag coefficient still remains high although some reduction is obtained when compared to that of the basic model.

2) Type B: When the strakes are moved slightly inwards, as in the case of optimum configuration, the separated shear layer reattaches smoothly at or close to the corners of the flat-faced noncircular cylinder as sketched in Fig. 7b. This phenomenon can be clearly seen in the photograph of Fig. 4d. It is further evidenced by the steep pressure rise (Fig. 3d) that is characteristic of turbulent reattachment, suggesting that the flow transition may have occurred in the separated shear layer prior to reattachment. However, it is possible that there may be a lower limit on the freestream Reynolds number below which the transition in the separated shear layer prior to reattachment may not take place. This fact was not explored here.

The reattached flow continues smoothly along the model surface to some extent before eventually separating once again around $\theta = 120$ deg/140 deg. With this flow pattern, the vortex shedding is very much suppressed and the time-averaged (mean) base pressure displays a remarkable recovery (Fig. 5) resulting in a sharp decrease of drag coefficient (Fig. 6). For bluff bodies, such a flow pattern typically occurs at supercritical Reynolds numbers. Noting that the critical Reynolds num-

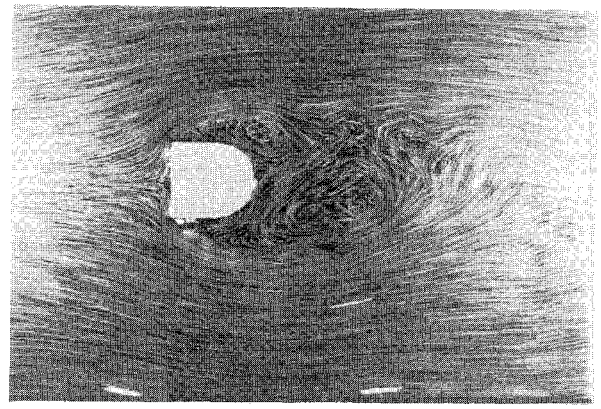

a) Basic model

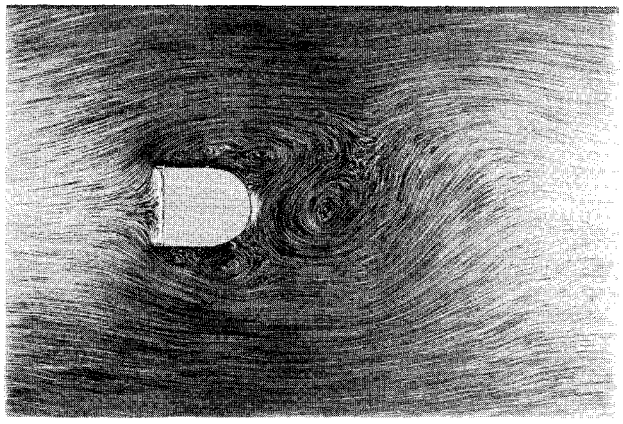

b) $\eta = 0$ $\xi = 0.1$

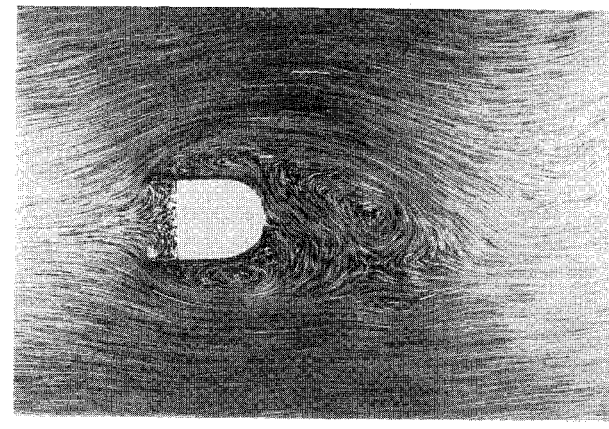

$\xi = 0.3$

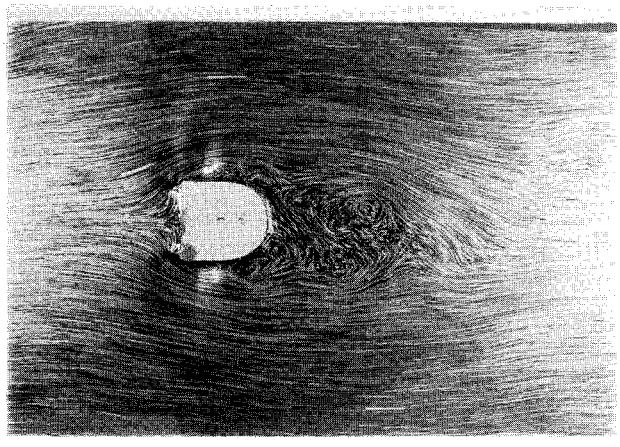

c) $\eta = 0.1$ $\xi = 0.1$

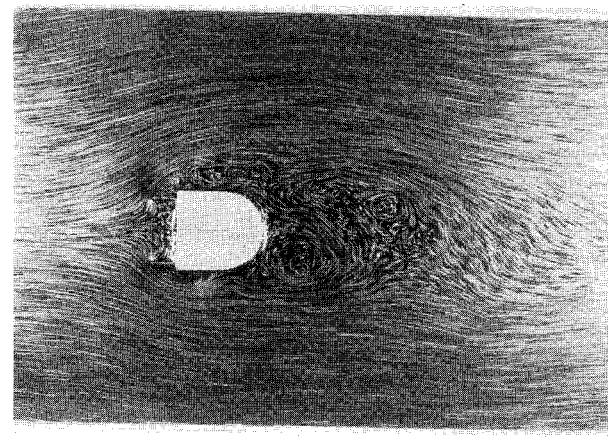

$\xi = 0.3$

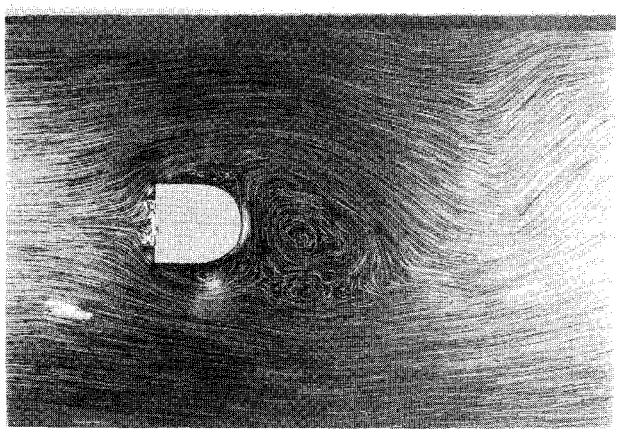

d) $\eta = 0.2$ $\xi = 0.1$

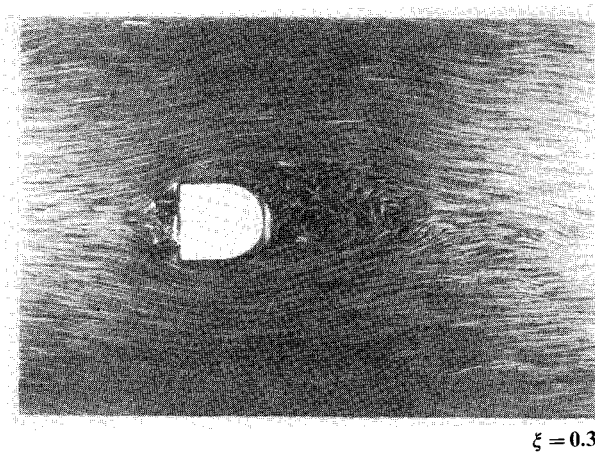

$\xi = 0.3$

Fig. 4 Flow visualization photographs for basic model and various strake configurations.

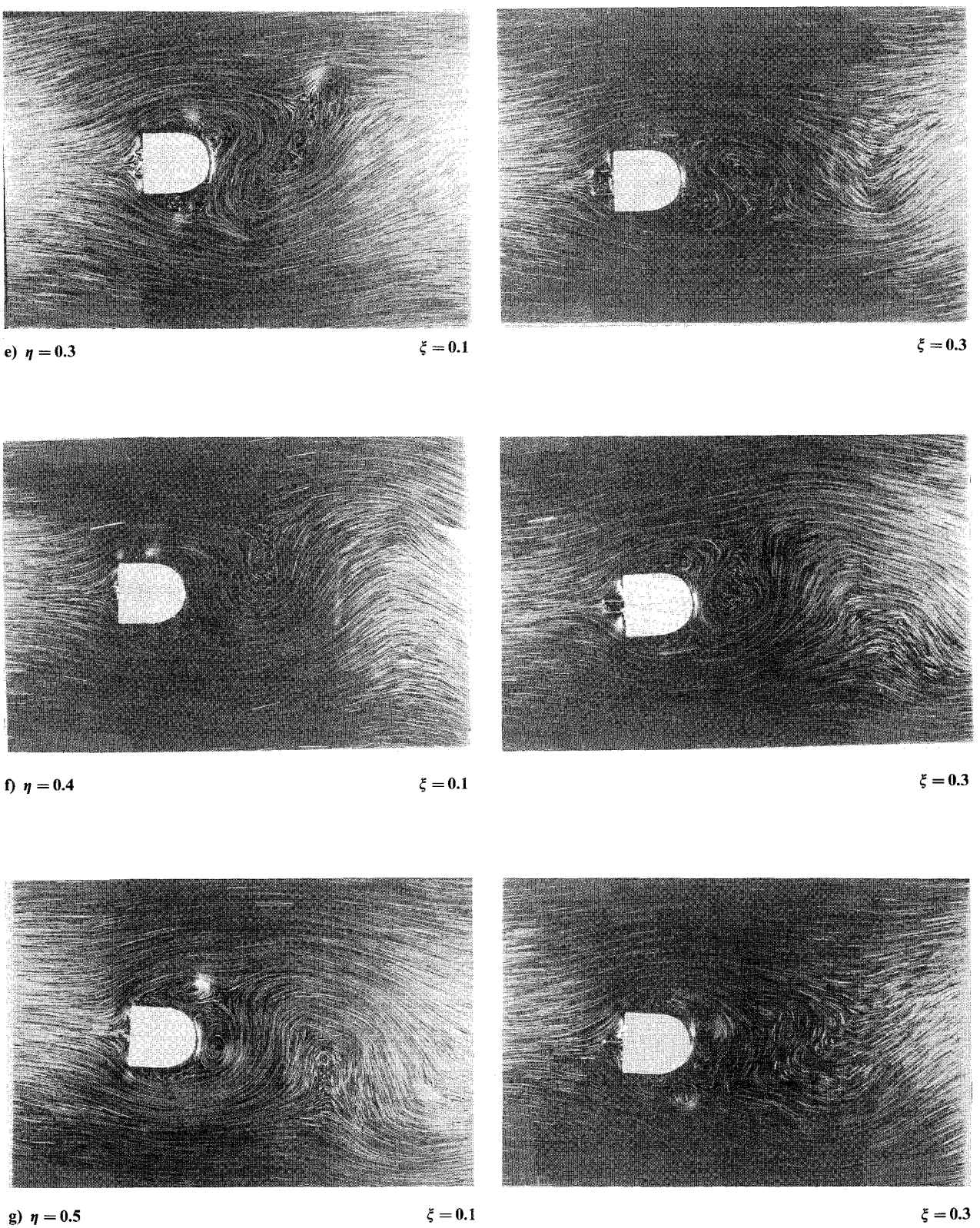

Fig. 4 Continued (flow visualization photographs).

ber for the subject cross section[2] is in excess of 4×10^6, we may state that this particular (optimum) strake configuration has accelerated the transformation in the flow pattern from subcritical to supercritical type as seen from the pressure distributions presented in Fig. 8 (reproduced from Fig. 3). This flow is further characterized by smooth reattachment of the separated shear layer at or close to the corners of the flat-faced cylinder. In Fig. 8 the sub- and supercritical pressure distribution over circular cylinder[6] is included for relative comparison.

3) Type C: With further inward movement of strakes ($0.2 < \eta < 0.5$) the separated shear layer reattaches on the flat face of the cylinder but cannot negotiate the sharp corners and separates at the corners, forming a large wake (Fig. 9). Once again, strong, alternating, and periodic vortex shedding occurs in the wake that is characterized by a high degree of coherence. The base suction is high and the drag coefficient increases and returns to the value of basic model as seen for the strake location of $\eta = 0.5$.

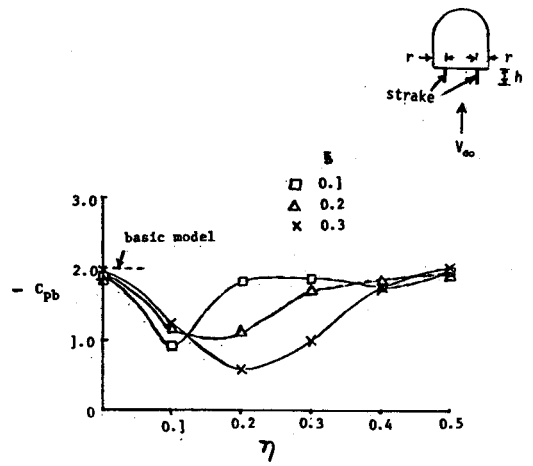

Fig. 5 Base pressure variation for various strake configurations.

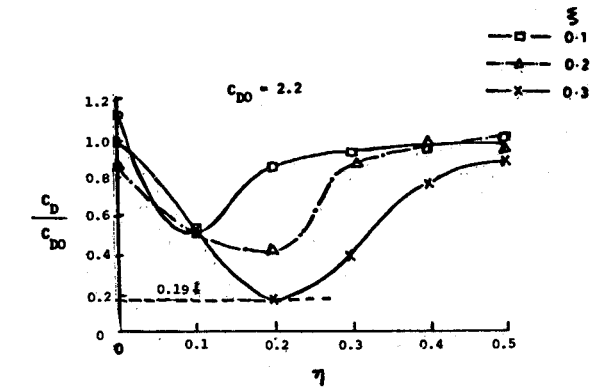

a) Variation of drag coefficient

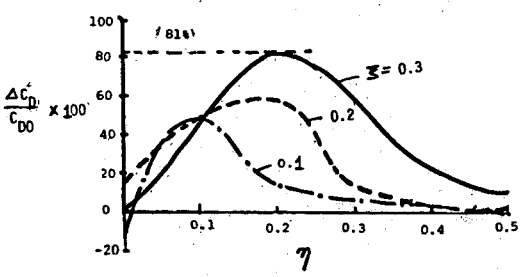

b) Percentage drag reduction

Fig. 6 Effect of strakes on drag coefficient.

The above flow patterns (A, B, and C) have a close resemblance to the study of Koenig and Roshko[4] who investigated the effect of a forward-facing circular disk on the forebody drag of a flat-faced, axially symmetrical semi-infinite cylinder. In the absence of the disk, the forebody drag coefficient was around 0.78. This drag force mainly arises due to the positive pressure acting on the flat face. Koenig and Roshko systematically varied the ratio of the diameters of the disk and the semi-infinite flat-faced cylinder as well as the gap between these two bodies. They found that a drastic decrease in the forebody drag coefficient of the disk-cylinder combination occurred for each diameter ratio at a certain gap. Values of C_D as low as 0.01, which are close to the theoretical value of zero as predicted by Prandtl and Tietjens,[5] were obtained. For this optimum condition, they observed that the shear layer separating from the sharp corners of the disk smoothly reattached at or near the shoulder of the semi-infinite cylinder. For other configurations, the reattachment of the shear layer originating

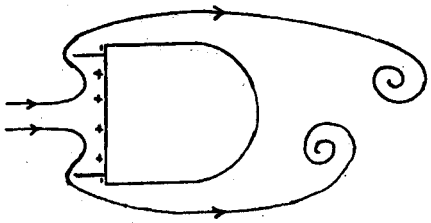

a) Strakes close to the corners ($\eta = 0$ and 0.1)

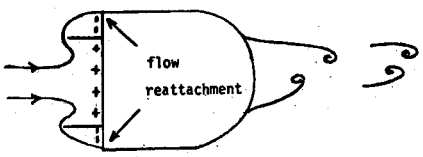

b) Optimum strake configuration ($\xi = 0.3$, $\eta = 0.2$)

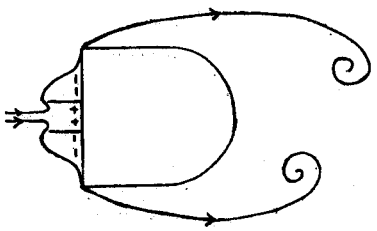

c) Strakes close to the center ($\eta = 0.3$–0.5)

Fig. 7 Schematic sketches of flow patterns around the model with various strake configurations.

at the edges of the disk either occurred on the flat face or downstream of the shoulder. When such flow pattern occurred, the associated drag coefficients were much higher than the minimum value. Thus, the close similarity of the flow patterns associated with the drastic drag reduction of flat-faced cylinders between the present study and that of Koenig and Reshko, in spite of differences in model geometry, Reynolds number, and nature of the flow (two-dimensional in the present study and axially symmetrical in the case of Koenig and Roshko[4]) suggests that the primary mechanism is the smooth reattachment of the separated shear layer at or close to the corner/shoulder of the flat-faced cylinder.

Another additional factor that contributes towards drag reduction and believed to be a novel feature of the present technique is the generation of significant suction over the windward face. This phenomenon appears to be strongly dependent on the strake location. With strakes on the windward face, the positive pressures are confined only to the region bounded by the strakes. Between the strake and windward corners (region marked as Δs in Fig. 3) high suction is produced on account of sharp turning of the flow. This phenomenon can be observed from Figs. 3b to 3f for strake locations $\eta = 0.1$–0.4. These negative pressures contribute significantly to drag reduction and are responsible for the drastic fall in C_D below the value of 1.0 corresponding to circular cylinder. As noted earlier, circular cylinder represents the limiting case of corner-rounding technique.

Since the generation of the suction pressure over part of the windward face is associated with primary flow separation at the sharp edges of the strakes, surface finish and the Reynolds number may not be significant factors here. In other words, although the present investigation was conducted at low Reynolds numbers and on smooth models, it appears that this phenomenon of generation of suction over the windward face can be exploited even in high Reynolds number flows for bluff bodies with smooth or rough surfaces. However, further studies are necessary to shed more light on this problem.

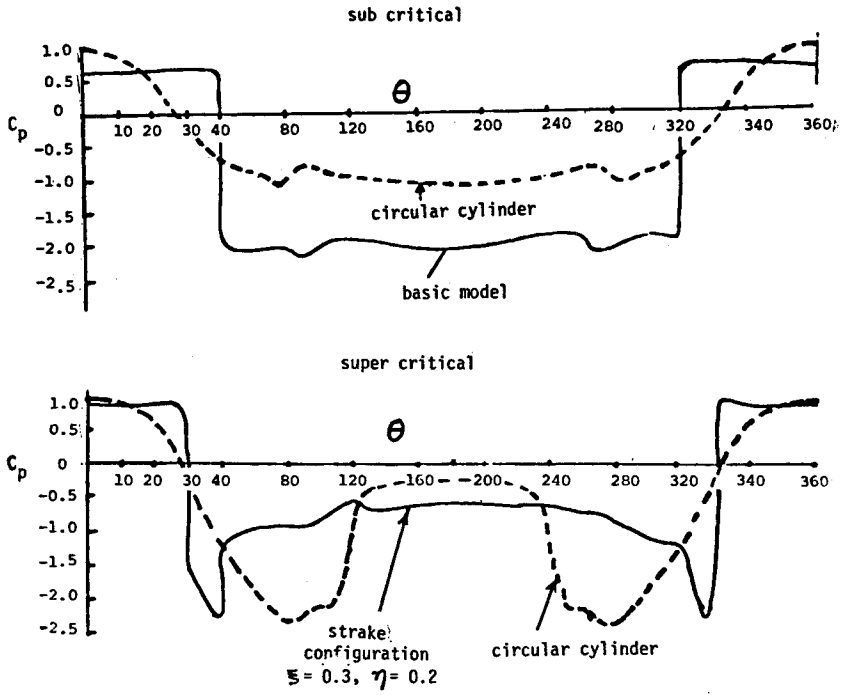

Fig. 8 Sub- and supercritical pressure distributions.

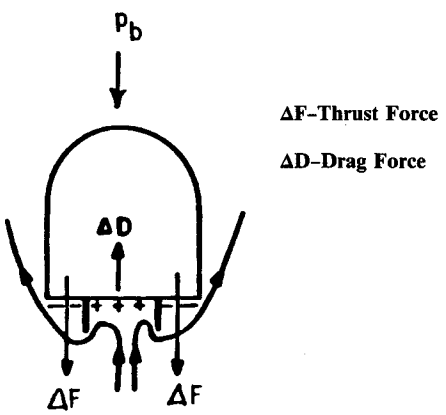

Fig. 9 Schematic sketch of flow pattern around the windward face of the model with strakes (ΔF = thrust force, ΔD = drag force).

Conclusions

The present technique of installation of strakes on the windward face is a powerful method of reducing the drag of sharp-cornered noncircular cylinders. Drag reductions of about 80% are found to be possible by this approach by locating strakes at optimum configurations. Further tests with strakes of larger heights ($h > 0.3\ b_o$) are necessary to determine the limiting values of drag reduction for the subject model. Effect of Reynolds number also needs to be explored.

The primary mechanisms leading to dramatic drag reduction are identified as 1) confining the positive pressures only to a part of the windward face between the strakes and forcing the flow to separate at the edges of the strake so as to generate large negative (suction) pressures over the remaining part of the windward face, and 2) smooth reattachment of the separated shear layer at or close to the corners of the flat-faced cylinder. In this fashion, the present technique represents an attempt to exploit the flow separation for beneficial effects of drag reduction.

References

[1]Hoerner, S. F., *Fluid Dynamic Drag*, Brick Town, New Jersey, 1965.

[2]Jorgensen, L. H. and Brownson, J. J., "Effect of Reynolds Number and Body Corner Radius on Aerodynamic Characteristics of a Space Shuttle-type Vehicle at Subsonic Mach Numbers, "NASA TN D-6615, 1972.

[3]Obasaju, E. D., "An Investigation of the Effects of Incidence on the Flow Around a Square Section Cylinder," *Aeronautical Quarterly*, Vol. 34, Nov. 1983, pp. 243–259.

[4]Koenig, K. and Roshko, A., "An Experimental Study of Geometrical Effects on the Drag and Flow Field of Two Bluff Bodies Separated by a Gap," *Journal of Fluid Mechanics*, Vol. 156, 1985, pp. 167–204.

[5]Prandtl, L. and Tietjens, O. G., *Applied Hydro and Aeromechanics*, (translated by J. P. Hartog), Dover, 1934. pp. 77–81.

[6]Schlichting, H., *Boundary Layer Theory*, McGraw-Hill, 6th ed., 1966, pp. 20–21.